HHS Public Access

Author manuscript

Shock. Author manuscript; available in PMC 2023 February 01.

Published in final edited form as:

Shock. 2022 February 01; 57(2): 274–280. doi:10.1097/SHK.0000000000001882.

Assessment of Protection Offered by the Nrf2 Pathway Against Hyperoxia-induced Acute Lung Injury in Nrf2 Knockout Rats

Said H. Audi[1,2], **Elizabeth R. Jacobs**[1,3], **Pardis Taheri**[1,2], **Swetha Ganesh**[1,2], **Anne V. Clough**[2,4]

[1]Marquette University-Medical College of Wisconsin Department of Biomedical Engineering

[2]Clement J. Zablocki V.A. Medical Center

[3]Division of Pulmonary and Critical Care Medicine, Medical College of Wisconsin

[4]Department of Mathematical and Statistical Sciences, Marquette University

Abstract

Nuclear factor erythroid 2-related factor (Nrf2) is a redox-sensitive transcription factor that responds to oxidative stress by activating expressions of key antioxidant and cytoprotective enzymes via the Nrf2-antioxidant response element (ARE) signaling pathway. Our objective was to characterize hyperoxia-induced acute lung injury (HALI) in Nrf2 knock-out (KO) rats to elucidate the role of this pathway in HALI. Adult Nrf2 wildtype (WT) and KO rats were exposed to room air (normoxia) or > 95% O_2 (hyperoxia) for 48 hours, after which selected injury and functional endpoints were measured *in vivo* and *ex vivo*. Results demonstrate that the Nrf2-ARE signaling pathway provides some protection against HALI, as reflected by greater hyperoxia-induced histological injury and higher pulmonary endothelial filtration coefficient in KO versus WT rats. We observed larger hyperoxia-induced increases in lung expression of glutathione (GSH) synthetase, 3-nitrotyrosine (index of oxidative stress), and interleukin-1β, and *in vivo* lung uptake of the GSH-sensitive SPECT biomarker ^{99m}Tc-HMPAO in WT compared to KO rats. Hyperoxia also induced increases in lung expression of myeloperoxidase in both WT and KO rats, but with no difference between WT and KO. Hyperoxia had no effect on expression of Bcl-2 (anti-apoptotic protein) or peroxiredoxin-1. These results suggest that the protection offered by the Nrf2-ARE pathway against HALI is in part via its regulation of the GSH redox pathway. To the best of our knowledge, this is the first study to assess the role of the Nrf2-ARE signaling pathway in protection against HALI using a rat Nrf2 knockout model.

Keywords

Acute Respiratory Distress Syndrome (ARDS); lung microvascular permeability; Single Photon Emission Computed Tomography (SPECT); hexamethylpropyleneamine oxime (HMPAO); myeloperoxidase (MPO); glutathione (GSH); interleukin-1β (IL-1β)

Corresponding Author: Said H. Audi, PhD, Research Service 151, Zablocki VA Medical Center, 5000 W. National Ave, Milwaukee, WI 53233, said.audi@marquette.edu, Phone: 414-384-2000 ext. 41452, FAX: 414-384-0115.

INTRODUCTION:

Acute lung injury (ALI) is one of the most frequent causes of admission to medical intensive care units (1, 2). ALI and its most serious form Acute Respiratory Distress Syndrome (ARDS) are characterized by rapidly progressing hypoxic lung failure and carry high morbidity. ALI is often triggered by overwhelming infections associated with sepsis or pneumonia, including that caused by COVID-19 (3). Even prior to COVID-19, ARDS occurred in ~250,000 patients/year in the U.S., carried a mortality rate that exceeded 40%, lacked early detection tools, and had limited therapies (1, 2). Ventilation with high concentrations of oxygen (hyperoxia) is required to maintain adequate oxygenation to systemic organs and tissues (4). However, sustained exposure to high fractions of oxygen causes or exacerbates ALI (5).

Oxidative stress, inflammation, and mitochondrial dysfunction are key pathways in the pathogenesis of ALI, with the pulmonary capillary endothelium a primary and early target (6–12). Nuclear factor erythroid 2-related factor (Nrf2) is a redox-sensitive transcription factor that responds to oxidative stress by activating the expression of key antioxidant and cytoprotective enzymes via the Nrf2-**a**ntioxidant **r**esponse **e**lement (ARE) signaling pathway (13, 14). As such, Nrf2 has been shown to regulate glutathione (GSH) biosynthesis, protect mitochondrial function, and inhibit apoptosis, all of which are pertinent to the pathogenesis of ALI (13–17).

Previous studies in mice have suggested that the Nrf2-ARE signaling pathway provides protection against acute lung injuries, including ARDS (18–22). Using Nrf2 knockout mouse strains, Cho et al. suggested that the Nfe212 gene, which encodes the Nrf2 transcription factor, diminishes susceptibility to hyperoxic lung injury (22). In another study, Cho et al. showed that Nrf2 knockout mice were more sensitive to hyperoxia (>95% O_2 for 72 hrs) than wild-type mice (18). Additionally, Reddy el al. demonstrated a role for Nrf2-regulated GSH synthesis not only in protection against hyperoxia-induced injury, but also in the resolution of lung injury following exposure to hyperoxia (20). These results suggest a protective role for Nrf2 against hyperoxic lung injury.

Priestley et al. developed a Nrf2 knock-out (KO) rat model (23). They reported that mRNA expression for catalase, HO-1, superoxide dismutase 1 and 2, and glutathione reductase in livers of KO rats were 35–55% lower than those in wild-type (WT) rats. The objective of the present study is to use the rat Nrf2 KO model to assess specific lung injury endpoints and the role of this pathway in protection against hyperoxia-induced ALI in rats. Nrf2 WT and KO rats were compared under normoxic and hyperoxic conditions using both *in vivo* molecular imaging to demonstrate alterations in the pulmonary oxidant status and *ex vivo* assays to determine changes in selected functional and structural endpoints. It is important to perform studies on the role of the Nrf2 pathway in hyperoxia-induced ALI (HALI) in this rat Nrf2 KO model since rats undergo a unique acclimation process during exposure to hyperoxia and develop tolerance to otherwise lethal hyperoxia that mice do not (24, 25). Moreover, the sequence of events leading to O_2 toxicity is best described in rats (5).

MATERIALS AND METHODS:

Materials:

HMPAO (Ceretec®) was purchased in kit form from GE Healthcare (Arlington Heights, IL), and technetium-labeled macroaggregated albumin (^{99m}Tc-MAA, particle sizes 20 – 40 μm) was purchased from Cardinal Health (Wauwatosa, WI). Antibodies were purchased from Abcam for GSH synthetase (cat # 124811), Bcl-2 (cat # ab59348), myeloperoxidase (MPO) (cat # ab188211), and 3-nitrotyrosine (3-NT) (cat # ab52309). Antibodies for interleukin-1β (IL-1β) and peroxiredoxin-1 (Prdx-1) were purchased from RD systems (cat # MAB5011) and Cell Signaling (cat # 8499), respectively.

Rat model of human ALI:

All treatment protocols were approved by the Institutional Animal Care and Use Committees of the Zablocki Veterans Affairs Medical Center, the Medical College of Wisconsin, and Marquette University.

Male littermate Sprague Dawley Nrf2 KO (SD-*Nfe212*^{em1Mcwi}) wildtype (WT) and homozygous (KO) rats were bred by and obtained from the Medical College of Wisconsin Rat Research Model Service Center as described by Priestley et al. (23). For normoxia (control) studies, adult (68–77 days old) WT and KO rats (321 ± 7 (SE) g, n = 25) were housed in chambers with room air. For hyperoxia studies, age- and weight-matched WT (331 ± 8 g, n = 18) and KO rats (332 ± 14 g, n = 17) were housed adjacent to the room-air chambers in exposure chambers with > 95% O_2 for 48 hrs, as previously described (26). This exposure period was chosen since it is relatively early in the pathogenesis of hyperoxia-induced ALI, prior to clinical evidence of respiratory distress (5, 26, 27). Four groups of rats were studied: WT normoxia, WT hyperoxia, KO normoxia and KO hyperoxia.

Lung wet-to-dry weight ratio, weight of pleural effusion:

Heart and lungs from a randomly selected subset of each group of rats were isolated as previously described (26). The lungs were dissected free of the heart, trachea and mainstem bronchi and total lung wet weight was obtained. The left lung lobe was weighed and dried at 60°C for 72 hrs for wet-to-dry weight ratio and the remaining lung lobes were used for histological studies described below (26). For a subset of rats exposed to hyperoxia, cotton gauze was inserted into the chest cavity to absorb any pleural effusion (28). The gauze was weighed before and after use and the difference in weights was determined.

Histology:

In a randomly selected subset of rats from each group, excised lungs were fixed after inflation in 10% neutral buffered formalin (Fisher Scientific, Pittsburg, PA) and embedded in paraffin. Whole-mount sections of lung were cut (4 μm thick), processed and stained with Hematoxylin & Eosin (H&E, Richard Allan, Kalamazoo, MI). Using high resolution jpeg images of the slides, an investigator masked to the treatment groups obtained 3–5 representative images from pre-selected areas of the lung on each slide, avoiding large vessels or airways at 100X (for neutrophils and edema) and 400X (for alveolar septum thickness). These images were then scored for injury independently and values for each rat

averaged for a single “n”. We used a 0–2 scoring system suggested by Matute-Bello et al. (29) for neutrophil influx, edema, and thickness of the diffusion barrier (Table 1).

Western blots:

Western blot analysis was carried out as previously described (30) on whole lung tissue homogenate to quantify the expressions of glutathione (GSH) synthetase as an indicator of the GSH redox pathway, the anti-apoptotic protein Bcl-2, and pro-inflammatory cytokine interleukin-1β (IL-1β) (for electrophoresis, protein used was 40 μg/lane). For myeloperoxidase (MPO), as an indicator of inflammation, and the anti-oxidant peroxiredoxin 1 (Prdx-1), 45 μg/lane protein was loaded. Western blot analysis was also carried out on whole lung tissue homogenate (protein concentration 30 μg/μl) to quantify the expression of 3-nitrotyrosine (3-NT) as an indicator of oxidative stress (27).

Pulmonary vascular endothelial filtration coefficient (K_f):

Randomly selected rats from normoxia and 48-hr hyperoxia WT and KO groups were anesthetized with pentobarbital sodium (50–100 mg/kg i.p.). The lungs were then removed and suspended from a calibrated force displacement transducer (ModelFT03; Grass Instruments), attached to a rat lung ventilation-perfusion system, and lung weight was monitored continuously (26, 31). The value of K_f, a measure of vascular permeability, was then determined using the approach described by Bongard et al. (31). Briefly, after a 10 min stabilization period with the venous pressure (P_V) set at atmospheric pressure, P_V was raised to 3.7 mmHg and the lung perfused for 10 min. Then, P_V was raised to 10 mmHg and perfusion continued for an additional 10 min. K_f was determined by dividing the difference in the rate of lung weight gain measured 10 min after increasing P_V from 3.7 to 10 mmHg and after increasing P_V from 0 to 3.7 mmHg by the difference in pulmonary capillary pressure at these P_V values. For each P_V, the capillary pressure was estimated as the average of arterial and venous pressures. K_f was normalized to gram of dry lung weight.

Imaging studies:

In vivo imaging studies described below were conducted on randomly selected subsets of rats from each group. Sample sizes were chosen to achieve a power ≥ 85% using power analysis (ANOVA power) based on previously published means and standard deviations of the lung uptake of ^{99m}Tc-HMPAO (26, 28, 32).

^{99m}Tc-HMPAO was constituted and labeled according to kit directions as previously described (26, 28). Rats were anesthetized with sodium pentobarbital (40–50 mg/kg, i.p.) and a tail vein was cannulated. The rat was then placed supine on a plexiglass plate (4 mm) positioned directly on the face of a parallel-hole collimator (hole diameter = 2 mm, depth = 25 mm) attached to a modular gamma camera (*Radiation Sensors, LLC*) for planar imaging (26, 28). An injection (37–74 MBq) of ^{99m}Tc-HMPAO was administered via the tail vein catheter. ^{99m}Tc-HMPAO reaches steady-state in the lung by 20 minutes post-injection, at which time 3 thirty-second planar images were acquired (26, 28).

A subsequent injection of ^{99m}Tc-MAA (37 MBq) was made via the same tail-vein cannula and the rat re-imaged. The ^{99m}Tc-MAA injection provided a planar image in which the lung

boundaries were clearly identified, since >95% of ^{99m}Tc-MAA lodged in the lungs. After imaging, the rats were euthanized with an overdose of pentobarbital.

Image analysis:

Images were analyzed using MATLAB-based software developed in-house. The boundaries of the upper portion of the lungs were identified in the high-sensitivity ^{99m}Tc-MAA images and manually outlined to construct a lung region of interest (ROI) free of liver contribution (26). The ^{99m}Tc-MAA lung ROI mask was then superimposed on the ^{99m}Tc-HMPAO image yielding a lung ^{99m}Tc-HMPAO ROI. No registration was required since the animal was maintained in the same location throughout the imaging study. Background regions in the upper forelimbs were also identified in the ^{99m}Tc-HMPAO image to normalize lung activity for injected ^{99m}Tc-HMPAO specific activity, dose, and decay (26, 28). Mean counts/sec/pixel/injected dose within both the lung and forelimb-background ROIs were then determined and decay corrected. The ratio of the lung and background ROI signals averaged over the 3×30 second time interval, when the ^{99m}Tc-HMPAO signal within the ROIs had reached steady state, was used as the measure of lung ^{99m}Tc-HMPAO uptake (26, 28).

Statistical analysis:

Statistical evaluation of data was carried out using SigmaPlot version 12.0 (Systat Software Inc., San Jose, CA). Results are expressed as means ± SE unless stated otherwise. To evaluate differences between two groups of rats, an unpaired two-tailed *t*-test was used with the level of statistical significance set at 0.05.

RESULTS:

Lung wet/dry weight ratios, pleural effusion, and K_f

Rat exposure to hyperoxia for 48 hrs increased lung wet/dry weight ratio in both WT and KO groups and the increase was not different between WT and KO groups (Table 2). No pleural effusion was observed in either group of normoxic rats. Pleural effusions were identified in both of the hyperoxia cohorts, but no differences between the WT and KO groups were observed (Table 2).

The lung vascular endothelial filtration coefficient (K_f) was elevated in both the WT and KO rats after 48 hrs of hyperoxia (Figure 1) compared to normoxia. However, the hyperoxia-induced increase in K_f was ~50% greater in the KO group than the WT group.

Histology

Images of representative lung sections stained with H&E appear in Figure 2. Images from WT normoxia (A) and KO normoxia (B) rats show the expected lacy architecture of the lungs. The results (Table 3) show a higher overall histology score for the hyperoxic KO lungs than for hyperoxic WT lungs. This reflects the higher edema score in the KO group, with no difference in the neutrophilic influx or alveolar septum thickness scores between the hyperoxic WT and KO groups.

Western blots

Expression of MPO increased with hyperoxia in both WT and KO rats (Table 2), however the increase was not different between WT and KO rats. The measured hyperoxia-induced increases in MPO lung expression in both WT and KO rats (Table 2) are consistent with the increases in the neutrophilic influx histological scores (Table 3). Table 2 also shows that the hyperoxia-induced increases in both 3-NT and cytokine IL-1β expressions, relative to normoxic values, were larger in KO rats than in WT rats.

Table 4 shows that expression of GSH synthetase was elevated following 48 hrs of exposure to hyperoxia in WT rats, but not in KO rats. Expressions of Bcl-2 and Prdx-1 were not elevated following exposure to hyperoxia in either the WT or KO groups (Table 4).

Imaging results

Lung uptake of ^{99m}Tc-HMPAO was quantified from the biomarker images in groups of WT and KO rats exposed to either normoxia or hyperoxia. Figure 3 shows lung uptake (the ratio of lung-to-background signal at steady-state) of ^{99m}Tc-HMPAO in all four groups of rats studied. One-way ANOVA using the Holm-Sidak method was used to evaluate differences between means of the four groups. ^{99m}Tc-HMPAO uptake was ~120% greater in WT hyperoxia rats compared to WT normoxia rats, consistent with our previously published results in Sprague Dawley rats (26, 27). ^{99m}Tc-HMPAO uptake was modestly increased in KO hyperoxia rats compared to KO normoxia; this increase was not significant and was 72% smaller than the increase with hyperoxia in the WT group.

DISCUSSION:

The transcription factor Nrf2, which is constitutively localized mainly in the cytosol, translocates to the nucleus in response to oxidative stress, where it up-regulates a wide range of cytoprotective genes via the anti-oxidant response element (ARE) signaling pathway. As such, the Nrf2-ARE signaling pathway is a positive regulator of many cytoprotective genes, including those that encode for antioxidant enzymes (e.g., GSH system), anti-inflammatory enzymes (e.g., hemeoxygenase1), anti-apoptotic proteins (e.g., Bcl-2), and phase II detoxifying enzymes (e.g., NQO1), and is a key regular of redox homoeostasis (13–15, 33). The objective of this study was to assess the role of the Nrf2-ARE signaling pathway in protection against hyperoxia-induced acute lung injury (HALI) using Nrf2 KO rats. The results are the first to demonstrate that the Nrf2-ARE signaling pathway provides some protection against lung injury in rats exposed to hyperoxia for 48 hrs, as reflected by greater hyperoxia-induced histological injury, higher filtration coefficient, and higher hyperoxia-induced increases in lung expressions of 3-NT and IL-1β in KO rats compared to WT rats. Other novel aspects of this study include the use of SPECT imaging to track the protection offered by the Nrf2 pathway against HALI *in vivo*, and the assessment of the protective role of this pathway against any hyperoxia-induced increase in pulmonary vascular endothelial filtration coefficient, a measure of vascular permeability, in isolated perfused lungs.

The SPECT biomarker ^{99m}Tc-HMPAO was originally developed as a brain perfusion agent but its uptake and retention in several tissues serves as a marker of tissue redox state (26, 34). We have previously shown that in the lung, ^{99m}Tc-HMPAO reduction and thus its cellular retention, is strongly dependent on the oxidoreductive state of the tissue including intracellular GSH content. This is evidenced by a strong correlation between ^{99m}Tc-HMPAO lung uptake and lung tissue GSH content under a range of experimental conditions including duration of exposure to hyperoxia, mild and severe ALI resulting from intratracheal instillation of lipopolysaccharide, and treatment of HALI with hydrogen therapy (26, 27). One of our long-term goals is to use SPECT imaging for early detection of clinical ALI and for stratifying the risk of ARDS development in hosts with risk factors for ARDS. Knockout models such as Nrf2 provide a platform for assessing differences in key cellular processes that make a host more or less likely to develop ARDS. The measured differences in lung uptake of HMPAO *in vivo* between Nrf2 KO and WT rats following exposure to hyperoxia could be reflective of the protection offered by the Nrf2 pathway against hyperoxia-induced ALI. These results may have prognostic value in terms of early detection of ALI and/or for stratifying the risk of ARDS development in patients with risk factors for ARDS.

This study also reported higher lung expression of GSH synthetase and higher *in vivo* lung uptake of the GSH-sensitive SPECT biomarker HMPAO in WT compared to KO rats. These results suggest a larger hyperoxia-induced increase in the lung GSH redox pathway in Nrf2 WT rats compared to KO rats, suggesting that protection offered by the Nrf2-ARE signaling pathway against HALI is via the Nrf2-regulated GSH redox pathway (20). Further evidence of protection of the capillary-alveolar barrier is suggested by the lower values of the edema histological scores (Table 3) and K_f (Figure 1) in hyperoxic WT relative to hyperoxic KO lungs.

We and other have measured reduced (GSH) and oxidized (GSSG) forms of glutathione content of lung tissue homogenates (24, 35–37). Results showed that ~99% of lung tissue glutathione content is in the GSH form, with a GSH:GSSG ratio of > 100 under various experimental conditions (24, 35–37). In fact, the lung tissue GSSH content is low enough that in some conditions it was lower than the detection limit of the assay (24). As such, GSH/GSSH is not a sensitive or accurate measure of pulmonary oxidative stress. Instead, for the present study we measured lung tissue expression of 3-NT as an index of oxidative stress. Results (Table 2) show higher hyperoxia-induced increases in lung expressions of 3-NT in KO rats compared to WT rats. Curiously, normoxic Nrf2 WT lung tissue had higher expressions of 3-NT and IL-1β than normoxic Nrf2 KO lung tissue (Supplemental Digital Content). Some sort of compensatory responses to shifts in pro- and anti-oxidant defense stress proteins in the KO relative to WT rats is possible, but is beyond the scope of the present work.

Previous studies using genetically-modified mice have suggested that the Nrf2-ARE signaling pathway provides protection against HALI (18–22). Reddy et al. showed that after 48 hrs of hyperoxia, the expressions of Gclc glutamate-systeine catalytic subunit (a key enzyme for GSH biosynthesis) and GSH peroxidase were increased significantly in WT compared to normoxia mice, but not in KO mice (20). Consistent with these results, they

reported that total lung GSH levels increased with hyperoxia in WT mice but decreased in KO mice (20). Cho et al. reported that the lung expression of GSH S transferases (GST-Ya) increased more in Nrf2 WT mice than KO mice following exposure to hyperoxia for 72 hrs as compared to normoxia (18). Furthermore, they showed that lung expression of GSH peroxidase increased more in Nrf2 WT mice than in KO mice following exposure to hyperoxia (18). Those results are consistent with results of the present study in rats which show a hyperoxia-induced increase in the lung expression of GSH synthetase (Table 4) and in the lung uptake of the GSH-sensitive SPECT biomarker HMPAO (Figure 3) in Nrf2 WT, but not KO, rats. Furthermore, the results of the present study suggest less HALI in WT rats than Nrf2 KO rats, consistent with results from a previous study regarding a role for the Nrf2-regulated GSH redox pathway in the protection offered by the Nrf2-ARE signaling pathway against HALI (20).

Reddy et al. showed histological evidence of hemorrhage and alveolar damage in lungs of both Nrf2 WT and KO mice following exposure to hyperoxia for 48 hrs, but the injury endpoints and lung wet-to-dry weight ratios were not different between Nrf2 WT and KO mice (20). TUNEL staining supported an increase in cell death in both WT and KO mice with hyperoxia, but the difference between WT and KO was not significant (20). On the other hand, the lung expression levels of the pro-inflammatory cytokine interleukin 6 (IL-6) increased significantly in WT mice with hyperoxia, compared to a smaller increase in KO mice. These results are generally consistent with results in the present study in rats (Table 2–4).

Although there is evidence that Nrf2-regulated GSH synthesis offers protection against hyperoxia-induced injury and plays a role in the resolution of lung injury following exposure to hyperoxia, the mechanism of this protection is not well understood. Oxidative-stress induced mitochondrial dysfunction plays a key role in the pathogenesis of HALI (31, 38–45). The Nrf2-ARE pathway could protect mitochondria from oxidative stress associated with HALI via its effect on GSH synthesis (13, 14). As a regulator of cellular redox homeostasis, Nrf2 has an important effect on mitochondrial function (14, 17, 46). Previous studies reported a decrease in basal cellular respiration and mitochondrial ATP production as well as mitochondrial membrane potential depolarization in cells from Nrf2 knockout mice and an increase in cells from Kelch-like ECH-associated protein 1 (Keap1) knockout mice, where Keap1 is a cytoplasmic protein that acts as an inhibitor of Nrf2 transcriptional function by binding at its N-terminal regulatory domain (13, 14, 17, 46). Holmstrom et al. suggested that these alterations are due to the role of Nrf2 in regulating substrate availability for mitochondrial respiration via its effect on genes that encode for glucose-6-phosphate dehydrogenase (G6PD), malic enzyme 1, isocitrate dehydrogenase 1, and enzymes of the pentose phosphate pathway (14, 17).

One limitation of the current study is that the model used is a global Nrf2 KO model. Thus, the observed increase in susceptibility of KO rats to hyperoxia as compared to WT rats could be due to injury to organs other than the lungs. However, high O_2 levels due to hyperoxia exposure are mostly limited to the lungs because of the small effect of plasma O_2 partial pressure (pO_2) on blood O_2 content above physiological pO_2 (47, 48). Nevertheless,

the global effect could be tested by adding Nrf2 back to the lung by viral-mediated gene transfer. Such studies are outside the scope of the present study.

The lung consists of 40 different resident cell types (49). In addition, other cell types (e.g., leukocytes) are recruited to the lungs following injury (5, 26, 27). For the present study, the results provide no direct information regarding the contributions of the different cell types to the measured increase in susceptibility to hyperoxia in KO rats. However, endothelial cells would be expected to dominate because of their large surface area and high fraction (~50%) of total cells in normal lungs (5). These cells are also a primary and early target of HALI (5, 7, 11, 28, 45, 50). Hyperoxia-induced cellular infiltration and edema could confound the interpretation of measured hyperoxia-induced changes in the expressions of various proteins (Tables 2 and 4) and other measurements (e.g., SPECT imaging) (Figure 3).

To the best of our knowledge, this is the first study to assess the role of the Nrf2-ARE signaling pathway in protection against ALI using this rat Nrf2 knockout model. We demonstrated that the Nrf2-ARE signaling pathway provides some protection against lung injury in rats exposed to hyperoxia. Our *in vivo* and *in vitro* results suggest a larger hyperoxia-induced increase in the lung GSH redox pathway in Nrf2 WT rats compared to KO rats, supporting protection offered by the Nrf2-ARE signaling pathway against HALI is via the Nrf2-regulated GSH redox pathway.

Supplementary Material

Refer to Web version on PubMed Central for supplementary material.

ACKNOWLEDGEMENTS

We thank Ms. Sushma Kaul and Ms. Ying Gao for their help with the experiments.

This work was supported by NIH 2R15HL129209-02 (Audi, Clough, Jacobs) and VA Merit Review Award BX001681 (Jacobs, Audi, Clough). The authors have no conflicts of interest.

REFERENCES:

1. Bellani G, Laffey JG, Pham T, Fan E, Brochard L, Esteban A, Gattinoni L, van Haren F, Larsson A, McAuley DF et al. Epidemiology, Patterns of Care, and Mortality for Patients With Acute Respiratory Distress Syndrome in Intensive Care Units in 50 Countries. Jama 315: 788–800, 2016. [PubMed: 26903337]
2. Matthay MA, and Zemans RL. The acute respiratory distress syndrome: pathogenesis and treatment. Annu Rev Pathol 6: 147–163, 2011. [PubMed: 20936936]
3. Fan E, Brodie D, and Slutsky AS. Acute Respiratory Distress Syndrome: Advances in Diagnosis and Treatment. JAMA 319: 698–710, 2018. [PubMed: 29466596]
4. Girardis M, Busani S, Damiani E, Donati A, Rinaldi L, Marudi A, Morelli A, Antonelli M, and Singer M. Effect of Conservative vs Conventional Oxygen Therapy on Mortality Among Patients in an Intensive Care Unit: The Oxygen-ICU Randomized Clinical Trial. Jama 2016.
5. Crapo JD, Barry BE, Foscue HA, and Shelburne J. Structural and biochemical changes in rat lungs occurring during exposures to lethal and adaptive doses of oxygen. Am Rev Respir Dis 122: 123–143, 1980. [PubMed: 7406333]
6. Bannerman DD, and Goldblum SE. Mechanisms of bacterial lipopolysaccharide-induced endothelial apoptosis. Am J Physiol Lung Cell Mol Physiol 284: L899–914, 2003. [PubMed: 12736186]

7. Reiss LK, Uhlig U, and Uhlig S. Models and mechanisms of acute lung injury caused by direct insults. Eur J Cell Biol 91: 590–601, 2012. [PubMed: 22284832]
8. Qiu X, Li H, Tang H, Jin Y, Li W, YuSun PingFeng, Sun X, and Xia Z. Hydrogen inhalation ameliorates lipopolysaccharide-induced acute lung injury in mice. Int Immunopharmacol 11: 2130–2137, 2011. [PubMed: 22015602]
9. Xie K, Yu Y, Huang Y, Zheng L, Li J, Chen H, Han H, Hou L, Gong G, and Wang G. Molecular hydrogen ameliorates lipopolysaccharide-induced acute lung injury in mice through reducing inflammation and apoptosis. Shock 37: 548–555, 2012. [PubMed: 22508291]
10. Chow CW, Herrera Abreu MT, Suzuki T, and Downey GP. Oxidative stress and acute lung injury. Am J Respir Cell Mol Biol 29: 427–431, 2003. [PubMed: 14500253]
11. Herrero R, Sanchez G, and Lorente JA. New insights into the mechanisms of pulmonary edema in acute lung injury. Ann Transl Med 6: 32, 2018. [PubMed: 29430449]
12. Kellner M, Noonepalle S, Lu Q, Srivastava A, Zemskov E, and Black SM. ROS Signaling in the Pathogenesis of Acute Lung Injury (ALI) and Acute Respiratory Distress Syndrome (ARDS). Adv Exp Med Biol 967: 105–137, 2017. [PubMed: 29047084]
13. Zhang M, An C, Gao Y, Leak RK, Chen J, and Zhang F. Emerging roles of Nrf2 and phase II antioxidant enzymes in neuroprotection. Prog Neurobiol 100: 30–47, 2013. [PubMed: 23025925]
14. Holmstrom KM, Kostov RV, and Dinkova-Kostova AT. The multifaceted role of Nrf2 in mitochondrial function. Curr Opin Toxicol 1: 80–91, 2016. [PubMed: 28066829]
15. Niture SK, and Jaiswal AK. Nrf2 protein up-regulates antiapoptotic protein Bcl-2 and prevents cellular apoptosis. J Biol Chem 287: 9873–9886, 2012. [PubMed: 22275372]
16. Metrailler-Ruchonnet I, Pagano A, Carnesecchi S, Ody C, Donati Y, and Barazzone Argiroffo C. Bcl-2 protects against hyperoxia-induced apoptosis through inhibition of the mitochondria-dependent pathway. Free Radic Biol Med 42: 1062–1074, 2007. [PubMed: 17349933]
17. Holmstrom KM, Baird L, Zhang Y, Hargreaves I, Chalasani A, Land JM, Stanyer L, Yamamoto M, Dinkova-Kostova AT, and Abramov AY. Nrf2 impacts cellular bioenergetics by controlling substrate availability for mitochondrial respiration. Biol Open 2: 761–770, 2013. [PubMed: 23951401]
18. Cho HY, Jedlicka AE, Reddy SP, Kensler TW, Yamamoto M, Zhang LY, and Kleeberger SR. Role of NRF2 in protection against hyperoxic lung injury in mice. Am J Respir Cell Mol Biol 26: 175–182, 2002. [PubMed: 11804867]
19. Chan K, and Kan YW. Nrf2 is essential for protection against acute pulmonary injury in mice. Proc Natl Acad Sci U S A 96: 12731–12736, 1999. [PubMed: 10535991]
20. Reddy NM, Kleeberger SR, Kensler TW, Yamamoto M, Hassoun PM, and Reddy SP. Disruption of Nrf2 impairs the resolution of hyperoxia-induced acute lung injury and inflammation in mice. J Immunol 182: 7264–7271, 2009. [PubMed: 19454723]
21. Kawamura T, Wakabayashi N, Shigemura N, Huang CS, Masutani K, Tanaka Y, Noda K, Peng X, Takahashi T, Billiar TR et al. Hydrogen gas reduces hyperoxic lung injury via the Nrf2 pathway in vivo. Am J Physiol Lung Cell Mol Physiol 304: L646–656, 2013. [PubMed: 23475767]
22. Cho HY, Jedlicka AE, Reddy SP, Zhang LY, Kensler TW, and Kleeberger SR. Linkage analysis of susceptibility to hyperoxia. Nrf2 is a candidate gene. Am J Respir Cell Mol Biol 26: 42–51, 2002. [PubMed: 11751202]
23. Priestley JR, Kautenburg KE, Casati MC, Endres BT, Geurts AM, and Lombard JH. The NRF2 knockout rat: a new animal model to study endothelial dysfunction, oxidant stress, and microvascular rarefaction. Am J Physiol Heart Circ Physiol 310: H478–487, 2016. [PubMed: 26637559]
24. Audi SH, Roerig DL, Haworth ST, and Clough AV. Role of Glutathione in Lung Retention of 99mTc-Hexamethylpropyleneamine Oxime in Two Unique Rat Models of Hyperoxic Lung Injury. J Appl Physiol 113: 658–665, 2012. [PubMed: 22628374]
25. Frank L, Iqbal J, Hass M, and Massaro D. New “rest period” protocol for inducing tolerance to high O2 exposure in adult rats. Am J Physiol 257: L226–231, 1989. [PubMed: 2801950]
26. Audi SH, Clough AV, Haworth ST, Medhora M, Ranji M, Densmore JC, and Jacobs ER. 99MTc-Hexamethylpropyleneamine Oxime Imaging for Early Detection of Acute Lung Injury in Rats

Exposed to Hyperoxia or Lipopolysaccharide Treatment. Shock 46: 420–430, 2016. [PubMed: 26974426]

27. Audi SH, Jacobs ER, Zhang X, Camara AK, Zhao M, Medhora MM, Rizzo B, and Clough AV. Protection by Inhaled Hydrogen Therapy in a Rat Model of Acute Lung Injury Can be Tracked in vivo Using Molecular Imaging. Shock 48: 467–476, 2017. [PubMed: 28915216]
28. Audi SH, Jacobs ER, Zhao M, Roerig DL, Haworth ST, and Clough AV. In vivo detection of hyperoxia-induced pulmonary endothelial cell death using (99m)Tc-duramycin. Nucl Med Biol 42: 46–52, 2015. [PubMed: 25218023]
29. Matute-Bello G, Downey G, Moore BB, Groshong SD, Matthay MA, Slutsky AS, and Kuebler WM. An official American Thoracic Society workshop report: features and measurements of experimental acute lung injury in animals. Am J Respir Cell Mol Biol 44: 725–738, 2011. [PubMed: 21531958]
30. Densmore JC, Jeziorczak PM, Clough AV, Pritchard KA, Jr., Cummens B, Medhora M, Rao A, and Jacobs ER. Rattus model utilizing selective pulmonary ischemia induces bronchiolitis obliterans organizing pneumonia. Shock 39: 271–277, 2013. [PubMed: 23364425]
31. Bongard RD, Yan K, Hoffmann RG, Audi SH, Zhang X, Lindemer BJ, Townsley MI, and Merker MP. Depleted energy charge and increased pulmonary endothelial permeability induced by mitochondrial complex I inhibition are mitigated by coenzyme Q1 in the isolated perfused rat lung. Free Radic Biol Med 65: 1455–1463, 2013. [PubMed: 23912160]
32. Clough AV, Audi SH, Haworth ST, and Roerig DL. Differential Lung Uptake of ^{99m}Tc-Hexamethylpropyleneamine Oxime and ^{99m}Tc-Duramycin in the Chronic Hyperoxia Rat Model. J Nucl Med 53: 1984–1991, 2012. [PubMed: 23086010]
33. Saha S, Buttari B, Panieri E, Profumo E, and Saso L. An Overview of Nrf2 Signaling Pathway and Its Role in Inflammation. Molecules 25: 2020.
34. Neirinckx RD, Burke JF, Harrison RC, Forster AM, Andersen AR, and Lassen NA. The retention mechanism of technetium-99m-HM-PAO: intracellular reaction with glutathione. J Cereb Blood Flow Metab 8: S4–12, 1988. [PubMed: 3192641]
35. Serrano-Mollar A, Closa D, Prats N, Blesa S, Martinez-Losa M, Cortijo J, Estrela JM, Morcillo EJ, and Bulbena O. In vivo antioxidant treatment protects against bleomycin-induced lung damage in rats. Br J Pharmacol 138: 1037–1048, 2003. [PubMed: 12684259]
36. Tipple TE, Welty SE, Rogers LK, Hansen TN, Choi YE, Kehrer JP, and Smith CV. Thioredoxin-related mechanisms in hyperoxic lung injury in mice. Am J Respir Cell Mol Biol 37: 405–413, 2007. [PubMed: 17575077]
37. Deneke SM, Gershoff SN, and Fanburg BL. Potentiation of oxygen toxicity in rats by dietary protein or amino acid deficiency. J Appl Physiol 54: 147–151, 1983. [PubMed: 6826398]
38. Sepehr R, Audi SH, Staniszewski KS, Haworth ST, Jacobs ER, and Ranji M. Novel Flurometric Tool to Assess Mitochondrial Redox State of Isolated Perfused Rat Lungs after Exposure to Hyperoxia. IEEE J Transl Eng Health Med 1: 2013.
39. Piantadosi CA, and Suliman HB. Mitochondrial Dysfunction in Lung Pathogenesis. Annu Rev Physiol 79: 495–515, 2017. [PubMed: 27959621]
40. Ten VS, and Ratner V. Mitochondrial bioenergetics and pulmonary dysfunction: Current progress and future directions. Paediatr Respir Rev 2019.
41. Du Q, Wang C, Zhang N, Li G, Zhang M, Li L, Zhang Q, and Zhang J. In vivo study of the effects of exogenous hydrogen sulfide on lung mitochondria in acute lung injury in rats. BMC Anesthesiol 14: 117, 2014. [PubMed: 25550681]
42. Ma C, Beyer AM, Durand M, Clough AV, Zhu D, Norwood Toro L, Terashvili M, Ebben JD, Hill RB, Audi SH et al. Hyperoxia Causes Mitochondrial Fragmentation in Pulmonary Endothelial Cells by Increasing Expression of Pro-Fission Proteins. Arterioscler Thromb Vasc Biol 38: 622–635, 2018. [PubMed: 29419407]
43. Patil SS, Hernandez-Cuervo H, Fukumoto J, Narala VR, Saji S, Borra M, Alleyn M, Lin M, Soundararajan R, Lockey R et al. Alda-1 attenuates hyperoxia-induced mitochondrial dysfunction in lung vascular endothelial cells. Aging (Albany NY) 11: 3909–3918, 2019. [PubMed: 31209184]

44. Zhang Y, Shan P, Srivastava A, Li Z, and Lee PJ. Endothelial Stanniocalcin 1 Maintains Mitochondrial Bioenergetics and Prevents Oxidant-Induced Lung Injury via Toll-Like Receptor 4. Antioxid Redox Signal 30: 1775–1796, 2019. [PubMed: 30187766]

45. Audi SH, Merker MP, Krenz GS, Ahuja T, Roerig DL, and Bongard RD. Coenzyme Q1 redox metabolism during passage through the rat pulmonary circulation and the effect of hyperoxia. J Appl Physiol 105: 1114–1126, 2008. [PubMed: 18703762]

46. Kovac S, Angelova PR, Holmstrom KM, Zhang Y, Dinkova-Kostova AT, and Abramov AY. Nrf2 regulates ROS production by mitochondria and NADPH oxidase. Biochim Biophys Acta 1850: 794–801, 2015. [PubMed: 25484314]

47. Mach WJ, Thimmesch AR, Pierce JT, and Pierce JD. Consequences of hyperoxia and the toxicity of oxygen in the lung. Nurs Res Pract 2011: 260482, 2011. [PubMed: 21994818]

48. Torbati D, Tan GH, Smith S, Frazier KS, Gelvez J, Fakioglu H, and Totapally BR. Multiple-organ effect of normobaric hyperoxia in neonatal rats. J Crit Care 21: 85–93; discussion 93–84, 2006. [PubMed: 16616630]

49. Kotton DN, and Morrisey EE. Lung regeneration: mechanisms, applications and emerging stem cell populations. Nat Med 20: 822–832, 2014. [PubMed: 25100528]

50. Merker MP, Audi SH, Lindemer BJ, Krenz GS, and Bongard RD. Role of mitochondrial electron transport complex I in coenzyme Q1 reduction by intact pulmonary arterial endothelial cells and the effect of hyperoxia. Am J Physiol Lung Cell Mol Physiol 293: L809–819, 2007. [PubMed: 17601793]

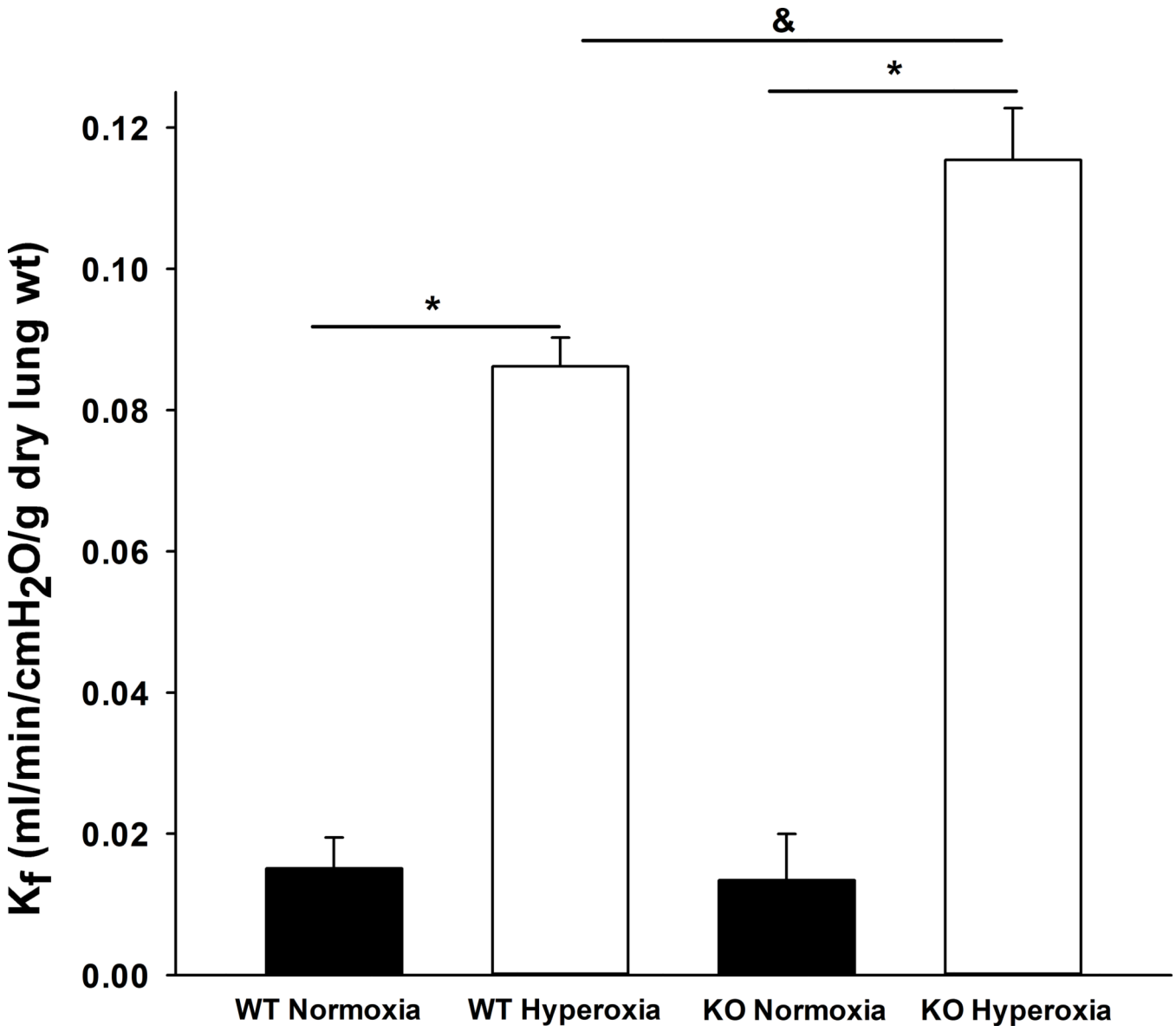

Figure 1:

Pulmonary vascular endothelial filtration coefficient, K_f, in lungs of wild-type (WT) and knockout (KO) rats exposed to normoxia or hyperoxia. * different between normoxia and hyperoxia. & different between WT hyperoxia and KO hyperoxia. n = number of rats: WT normoxia (4), WT hyperoxia (4), KO normoxia (3), KO hyperoxia (4).

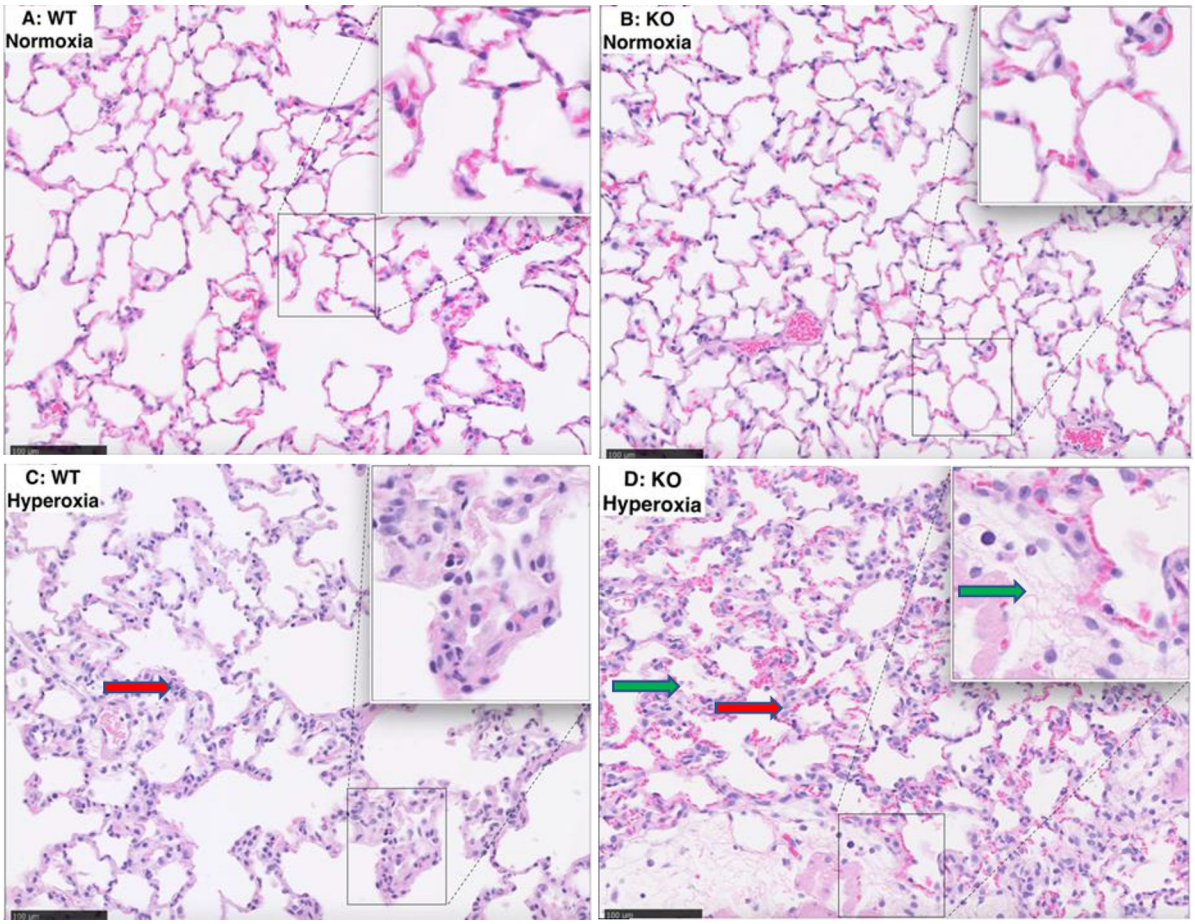

Figure 2:
Representative images of WT normoxia (A), KO normoxia (B), WT hyperoxia (C), and KO hyperoxia (D) H&E stained lungs slices. Scale is 100 μm.

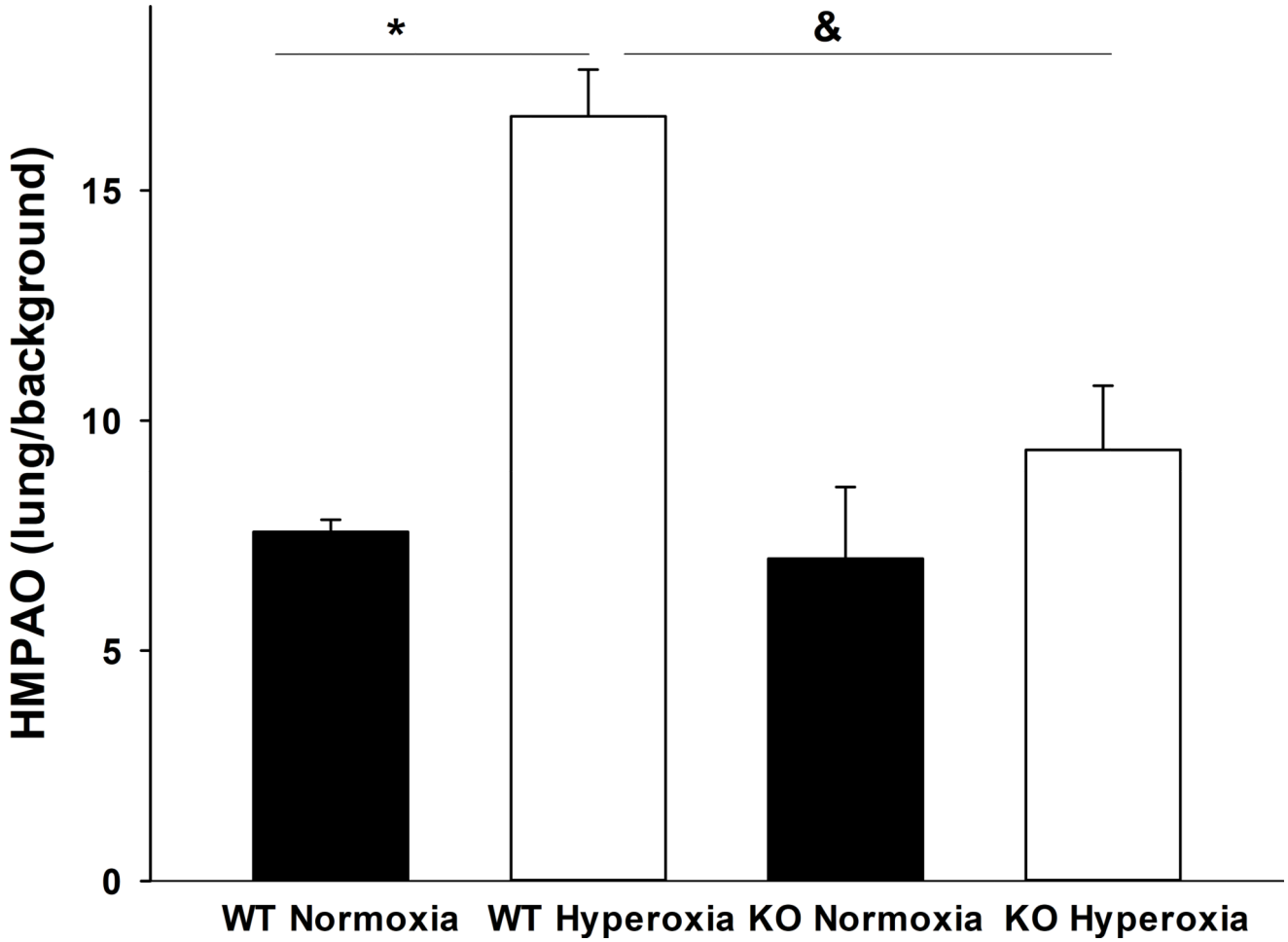

Figure 3:

Lung uptake of ^{99m}Tc-HMPAO in wild-type (WT) and knockout (KO) rats exposed to normoxia or hyperoxia. * different between WT normoxia and WT hyperoxia. $^{\&}$ different between WT hyperoxia and KO hyperoxia. n = number of rats: WT normoxia (3), WT hyperoxia (5), KO normoxia (5), KO hyperoxia (7).

Table 1:

Endpoints for histological injury grading on a scale of 0–2 for each injury.

Histology Injury endpoint/ score	0	1	2
Neutrophilic influx	None to very rare	Perivascular or peribronchiolar only	intra-alveolar and widely distributed
Edema	None to very rare	Proteinacious material in <5% and <20% field	proteinacious material in > 20% field
Thickness of alveolar septum	≤1.8 × control thickness	>1.8 but < 2.5 × control thickness	> 2.5 × control thickness

Table 2:

Injury endpoints

Group	Lung Wet/Dry wt	Pleural Effusion (g)	3-NT	MPO	IL-1β
WT normoxia	5.28 ± 0.21 (n = 12)	ND	1.0 ± 0.26 (n = 6)	1.0 ±0.27 (n = 6)	1.0 ± 0.17 (n = 6)
WT hyperoxia	6.07 ± 0.16 * (n =15)	3.53 ± 0.79 (n = 16)	2.45 ± 0.35 * (n = 6)	3.41 ± 0.36 * (n = 6)	1.92 ± 0.28 * (n = 6)
KO normoxia	5.35 ± 0.23 (n = 8)	ND	1.0 ± 0.36 (n = 4)	1.0 ± 0.28 (n = 3)	1.0 ± 0.32 (n = 4)
KO hyperoxia	5.96 ± 0.12 * (n = 17)	3.82 ± 1.02 (n = 14)	6.45 ± 1.67 *& (n = 6)	3.13 ± 0.37 * (n = 6)	4.95 ± 1.05 *& (n = 6)

3-NT, 3-nitrotyrosine; MPO, myloperoxidase; IL-1β, interleukin-1β. 3-NT, MPO, and IL-1β band density normalized to β actin and resulting values normalized to corresponding normoxia values. n = number of rats. ND = not detectable. Values are mean ± SE.

*different from normoxia

&different from WT hyperoxia (p <0.05).

Table 3:

Histological injury grading

Group	Total score	Neutrophilic influx	Edema	Thickness of alveolar septum
WT normoxia (n = 3)	0.05 ± 0.05	0.05 ± 0.05	0	0
WT hyperoxia (n = 6)	1.86 ± 0.26	1.17 ± 0.11	0.25 ± 0.14	0.44 ± 0.08
KO normoxia (n = 3)	0.11 ± 0.06	0	0	0.11 ± 0.06
KO hyperoxia (n = 6)	2.81 ± 0.09 *	1.28 ± 0.06	0.86 ± 0.10 *	0.67 ± 0.09

n = number of rats. Values are mean ± SE.

* different from WT hyperoxia (p <0.05).

Table 4:

Western blots of anti-oxidants and anti-apoptotic proteins

Group	Bcl-2	Prdx-1	GSH synthetase
WT normoxia	1.00 ± 0.13 (n = 6)	1.00 ± 0.04 (n = 6)	1.00 ± 0.18 (n = 6)
WT hyperoxia	1.14 ± 0.16 (n = 6)	1.03 ± 0.09 (n = 6)	1.76 ± 0.22 * (n = 6)
KO normoxia	1.00 ± 0.05 (n = 4)	1.00 ± 0.07 (n = 4)	1.00 ± 0.18 (n = 4)
KO hyperoxia	1.07 ± 0.14 (n = 6)	1.13 ± 0.09 (n = 6)	1.04 ± 0.09 (n = 6)

GSH, glutathione; Prdx-1, peroxiredoxin-1. Bcl-2, Prdx 1 and GSH synthetase band density normalized to β actin and resulting values normalized to corresponding normoxia values. n = number of rats. Values are mean ± SE.

* hyperoxia different from normoxia (p <0.05).